Send Orders for Reprints to reprints@benthamscience.net

Current Medical Imaging, 2021, *17*, 1010-1017

RESEARCH ARTICLE

Using the Compressed Sensing Technique for Lumbar Vertebrae Imaging: Comparison with Conventional Parallel Imaging

Tianyang Gao[1], Zhao Lu[1], Fengzhe Wang[1], Heng Zhao[1,2], Jiazheng Wang[3] and Shinong Pan[1,*]

[1]*Department of Radiology, Shengjing Hospital of China Medical University, Shenyang, Liaoning, China;* [2]*Department of Radiology, The First Affiliated Hospital of University of South China, Hunan, China;* [3]*Department of Clinical Science, Philips Healthcare, Beijing 100600, China*

ARTICLE HISTORY

Received: August 10, 2020
Revised: December 17, 2020
Accepted: December 22, 2020

DOI:
10.2174/1573405617666210126155814

Abstract: ***Objective*:** To compare conventional sensitivity encoding turbo spin-echo (SENSE-TSE) with compressed sensing plus SENSE turbo spin-echo (CS-TSE) in lumbar vertebrae magnetic resonance imaging (MRI).

***Methods*:** This retrospective study of lumbar vertebrae MRI included 600 patients; 300 patients received SENSE-TSE and 300 patients received CS-TSE. The SENSE acceleration factor was 1.4 for T1WI, 1.7 for T2WI, and 1.7 for PDWI. The CS total acceleration factor was 2.4, 3.6, 4.0, and 4.0 for T1WI, T2WI, PDWI sagittal, and T2WI transverse, respectively. The image quality of each MRI sequence was evaluated objectively by the signal-to-noise ratio (SNR) and contrast-to-noise ratio (CNR) and subjectively on a five-point scale. Two radiologists independently reviewed the MRI sequences of the 300 patients receiving CS-TSE, and their diagnostic consistency was evaluated. The degree of intervertebral foraminal stenosis and nerve root compression was assessed using the T1WI sagittal and T2WI transverse images.

***Results*:** The scan time was reduced from 7 min 28 s to 4 min 26 s with CS-TSE. The median score of nerve root image quality was 5 ($p > 0.05$). The diagnostic consistency using CS-TSE images between the two radiologists was high for diagnosing lumbar diseases ($\kappa > 0.75$) and for evaluating the degree of lumbar foraminal stenosis and nerve root compression ($\kappa = 0.882$). No differences between SENSE-TSE and CS-TSE were observed for sensitivity, specificity, positive predictive value, or negative predictive value.

***Conclusion*:** CS-TSE has the potential for diagnosing lumbar vertebrae and disc disorders.

Keywords: Lumbar vertebrae, nerve root, magnetic resonance imaging, compressed SENSE, turbo spin-echo, radiofrequency (RF).

1. INTRODUCTION

Lumbar vertebrae magnetic resonance imaging (MRI) is non-invasive and uses non-ionizing radiation. MRI has an important role in image analysis and is used widely for different purposes such as kidney segmentation [1, 2], liver segmentation [3], automated diagnosis systems [4], vessel segmentation [5, 6] or to evaluate low back pain quantitatively visualization of the dural sac, spinal cord, and nerve roots. However, the primary drawback of MRI is the speed of imaging. Although longer scan times increase the signal- to-noise ratio and resolution of the images, they also increase the procedural cost, patient waiting time, and the probability of motion artifacts in the images [7, 8].

Sensitivity encoding (SENSE) MRI acceleration is the method employed in clinical situations where the sensitivity profiles of multi-channel radiofrequency (RF) coils are exploited to shorten the gradient encoding procedure, reducing the imaging time [9]. Limitations in using SENSE and other parallel imaging techniques include a dependence on the number of receiver coils and the need for independent coil sensitivity profiles to avoid noise amplification of noise during the image reconstruction process.

Compressed sensing (CS) was introduced in 2006 by David Donoho [10] as a mathematical tool to accelerate imaging that was confirmed in MRI applications by Lustig *et al*. in 2007 [11]. CS is a k-space undersampling method that collects fewer data to preserve the quality of MR images [12]. CS utilizes the sparseness of MR imaging data and takes fewer measurements during image encoding steps in a pseudo-random manner, and then performs nonlinear optimization to reconstruct the undersampled data into an image having sufficient quality for clinical diagnosis [11, 13]. CS technology is built on CS theory and SENSE technology by balancing a variable density acquisition scheme and iterative reconstruction to solve inverse problems with a sparsity constraint [14]. Since its introduction, CS has significantly reduced scan times in multiple clinical imaging applications [15-19].

*Address correspondence to this author at the Department of Radiology, Shengjing Hospital of China Medical University, Shenyang, Liaoning, China; Tel: +86-8624-23929902; Email: cjr.panshinong@vip.163.com

This study aims to retrospectively compare the image quality and diagnostic accuracy between CS-TSE and SENSE-TSE in lumbar vertebrae MRI.

2. MATERIALS AND METHODS

2.1. Patient Population

We retrospectively enrolled 300 patients (male: female = 148:152; median age = 51 years; age range = 1–86 years) who received CS-TSE examinations from November 2017 to April 2018. During the same period, 300 patients (male: female = 149:151; median age: 51 years; age range: 2-87 years) who received SENSE-TSE examinations were also enrolled for comparison. All MR images were acquired on a 3.0 T MR scanner (Ingenia 3.0 T CX, Philips, Best, the Netherlands) equipped with a posterior in-built 44-channel spinal coil. This study was approved by the Ethics Committee of Shengjing Hospital of China Medical University, and the requirement for informed consent was waived.

2.2. Inclusion/exclusion Criteria

The inclusion criteria were as follows: patients with symptoms of low back pain and pain radiating to a lower extremity who received a lumbar MRI examination (SENSE-TSE or CS-TSE).

The exclusion criteria were as follows: patients with a history of lumbar surgery, pacemaker implantation, malignant tumor, infection, spinal malformations; patients with metal implants.

2.3. Examination Method

Scans were conducted with the patient supine and in a head-first position. Patients in both groups (SENSE-TSE and CS-TSE) were scanned in the T1WI sagittal, T2WI sagittal, T2WI transverse, and PDWI sagittal planes. SENSE-TSE scans were performed as reported [20]; the SENSE acceleration factor was 1.4 for T1WI, 1.7 for each T2WI plane, 1.7 for PDWI planes. The CS acceleration factor was 2.4 for T1WI sagittal, 3.6 for T2WI- and PDWI sagittal, and 4.0 for T2WI transverse planes. All imaging parameters are listed in Table **1**.

2.4. Image Quality Analysis

2.4.1. Signal-to-noise and Contrast-to-noise Ratios

Quantitative analysis of image quality was conducted using Philips Intellispace Portal. The region of interest (ROI) was drawn by a single radiologist (with 5 years' experience in spine MRI) on SENSE-TSE and CS-TSE images. ROIs were drawn in the lumbar centrum (L3), muscle (erector spinae), cerebrospinal fluid (CSF), and spinal cord. If there was an abnormality , the adjacent centrum was used for measurement. Nerve root ROIs were plotted on T1WI sagittal images. The ROI areas were as follows: L3, 20–25 mm2; muscle, 25–28 mm2; CSF, 5–7 mm2; spinal cord, 15–17 mm2; and nerve root, 2-3mm2. For SENSE-TSE and CS-TSE sequences, ROIs for each anatomical position were selected at approximately the same location or as close as possible between cases. ROIs were centered in the anatomical region as much as possible, with no lesions within the ROI. Representative ROIs are shown in Fig. (**1**).

Table 1. Magnetic resonance imaging parameters.

-	T1WI- Sagittal		T2WI- Sagittal		PDWI- Sagittal		T2WI-Axial	
-	**SENSE**	**CS**	**SENSE**	**CS**	**SENSE**	**CS**	**SENSE**	**CS**
TR/TE(ms)	569.00/6.00	569.00/6.00	2500.00/80.00	2500.00/80.00	2500.00/80.00	2500.00/80.00	2700.00/120.00	2700.00/120.00
FOV(mm)	160×312	160×312	160×312	160×312	160×312	160×312	170×170	170×170
Section thickness(mm)	4.0	4.0	4.0	4.0	4.0	4.0	4.0	4.0
Slice gap(mm)	0.4	0.4	0.4	0.4	0.4	0.4	0.4	0.4
Number of sections	12	12	12	12	12	12	12	12
Flip angle(deg.)	80	80	90	90	90	90	90	90
Sense factor	1.4	-	1.7	-	1.7	-	1.7	-
CS acceleration factor	-	2.4	-	3.6	-	3.6	-	4.0
Imaging time(s)	78	66	80	42	160	83	130	75

TR = Repetition time, TE = Echo time, FOV = Field of view.

Table 2. Subjective evaluation of image quality.

Score	Image Quality	Artifacts	Structures	Nerve Roots
1	Unacceptable	Severe artifact, obvious distortion	Heterogeneous, cannot be distinguished	Heterogeneous, cannot be distinguished
2	Worse than moderate,	Obvious artifact, mild distortion	Worse than moderate, Distinguishable but obscured	Worse than moderate, Distinguishable but obscured
3	Moderate	Moderate	Moderate	Moderate
4	Above moderate	Little artifact without obvious distortion	Mild heterogeneous, Blurry edged	Mild heterogeneous, Blurry edged
5	Excellent	No artifact	Homogeneous Clear and sharp edged	Homogeneous Clear and sharp edged

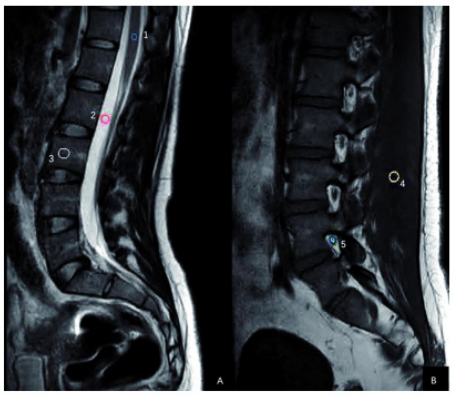

Fig. (1). Representative placements of regions of interest. **A**: CS-TSE-T2WI sagittal; **B**: CS-TSE-T1WI sagittal. ROI placements for the spinal cord (1), cerebrospinal fluid (2), bone marrow (3), muscle (4), and nerve root (5) are indicated. (*A higher resolution / colour version of this figure is available in the electronic copy of the article*).

Signal-to-noise ratios (SNRs) and contrast-to-noise ratios (CNRs) in images of centrum, muscle, CSF, spinal cord, and nerve root were calculated based on the ROIs. The SNR was obtained by dividing the average signal intensity (SI) by the standard deviation (SD) of the noise measured in the same ROI. The CNR was obtained by dividing the absolute value of the difference between the two tissue signal strengths by the SD of the noise. Two repeated measurements were taken at 2-week intervals. The formulas are as follows:

SNR=SI/SD,

CNR=(|SI_Tissue1-SI_Tissue2 |)/SD.

2.4.2. Subjective Evaluation of Image Quality

Two radiologists with more than five years' experience in musculoskeletal imaging scored the image quality of each SENSE-TSE and CS-TSE lumbar spine MRI (600 cases). Each evaluator was blinded to the image acquisition information. Each case was assigned a unique random number code and randomly assigned to each radiologist. The images were scored on a five-point scale for anatomic clarity, signal uniformity, and the appearance of artifacts in the centrum, muscle, and spinal cord [21] (Table **2**).

In T1WI sagittal images, two radiologists outlined the contours of nerve roots in the intervertebral foraminal. In T2WI transverse images, the morphology, edge definition, and signal uniformity of the L3-L4, L4-L5, and L5-S1 bilateral nerve roots were evaluated with a five-point scale [22] (Table **2**). Images having scores ≥ 3 were considered acceptable. To avoid recall bias, the first and second evaluations were conducted at least two weeks apart.

2.4.3. Evaluation of Disease Diagnosis Performance

After completing the subjective assessments, the same two radiologists independently analyzed the 300 CS-TSE cases to evaluate whether centrum fractures, degeneration, bone marrow changes, and spinal stenosis were present [22, 23]. The intervertebral disc was judged as protruding, bulging, prolapsed, or dissociated [24, 25]. The presence or absence of soft tissue swelling, tumors, or space-occupying lesions in the conus medullaris was also evaluated. Statistical analyses were conducted to measure the consistency between the two radiologists.

Two radiologists independently evaluated T1WI sagittal and T2WI transverse images from the 300 CS-TSE sequences for intervertebral foraminal stenosis and nerve root compression. Lumbar intervertebral foraminal stenosis and nerve root compression were classified according to the system proposed by Lee *et al*. [22] at L3-L4, L4-L5 and L5-S1. Statistical analyses were performed to measure the diagnostic consistency between the two radiologists.

Of the 600 cases, 145 SENSE-TSE and 161 CS-TSE cases were treated surgically. Sensitivity (Sen), specificity (Sep), positive predictive value (PV+), and negative predictive value (PV-) of the vertebral lesion, intervertebral disc, spinal canal disease, or soft tissue lesion diagnoses were calculated, using intraoperative diagnosis as the gold standard.

2.5. Statistical Analyses

Data were statistically analyzed using SPSS version 25.0 (SPSS Inc., Armonk, NY, USA). SNRs and CNRs of SENSE-TSE and CS-TSE sequences were compared using an independent-sample t-test, and repeated measurements were evaluated using analysis of variance (ANOVA). The subjective image quality scores from SENSE-TSE and CS-TSE sequences were compared using the Wilcoxon rank - sum test. Cohen's kappa coefficient was calculated to evaluate the diagnostic consistency from CS-TSE sequences for the degree of lumbar foraminal stenosis and nerve root compression. Values of $p < 0.05$ were considered statistically significant.

3. RESULTS

3.1. Quantitative Image Analysis

Using CS acceleration, the total scan time of lumbar vertebrae TSE was reduced from 7 min 28 s to 4 min 26 s, which represents a reduction of approximately 40% relative to that of SENSE-TSE. No significant differences in the SNRs of the centrum, muscle, CSF, and spinal cord regions were observed between SENSE-TSE and CS-TSE in T1WI, T2WI, and PDWI images ($p > 0.05$). However, the SNR in muscle was higher in T1WI and T2WI images from CS-TSE than from SENSE-TSE. No significant differences in the CNRs of the centrum, muscle, CSF, and spinal cord regions were observed between SENSE-TSE and CS-TSE ($p > 0.05$). CNRs of bone marrow-CSF, muscle-CSF, and spinal cord-CSF regions were higher in T2WI and PDWI images from CS-TSE than from SENSE-TSE. In T1WI images, no significant differences in the SNR or CNR of nerve root regions were observed between SENSE-TSE and CS-TSE ($p > 0.05$). SNR and CNR measurements from T1WI, T2WI, and PDWI images are shown in Table **3**.

Table 3. SNR and CNR values for TSE imaging of lumbar spine without and with CS.

-	T1WI			T2WI			PDWI		
	CS	SENSE	P-values	CS	SENSE	P-values	CS	SENSE	P-values
SNR(bone marrow)	15.50±4.30	15.58±4.18	0.977	16.17±3.20	16.80±8.83	0.885	7.33±1.58	10.21±3.48	0.131
SNR(muscle)	29.40±8.65	29.13±8.51	0.962	12.07±1.51	11.63±0.99	0.598	13.22±2.66	14.65±3.11	0.456
SNR(CSF)	10.55±3.13	13.14±2.54	0.188	72.20±8.51	67.41±7.55	0.374	51.11±4.80	52.30±5.74	0.731
SNR(spinal cord)	17.88±5.36	21.64±5.27	0.295	24.91±0.82	25.62±3.16	0.639	32.56±8.55	38.53±7.94	0.286
SNR(nerve root)	7.62±1.78	11.30±4.95	0.157	-	-	-	-	-	-
CNR(bone marrow /CSF)	9.36±2.93	9.58±2.35	0.900	27.97±7.60	25.80±8.66	0.686	37.05±7.68	34.01±5.38	0.489
CNR(muscle /CSF)	6.80±1.04	7.75±1.70	0.319	52.15±5.45	48.20±1.47	0.156	44.23±3.73	43.32±4.45	0.736
CNR(spinal cord /CSF)	6.03±2.22	10.02±3.86	0.080	37.15±3.18	35.12±2.75	0.312	31.68±4.31	29.79±2.46	0.419
CNR(nerve root /CSF)	2.63±0.97	4.06±2.07	0.201	-	-	-	-	-	-

SNR = signal-to-noise ratio, CNR = contrast-to-noise ratio, CSF = cerebrospinal fluid. The data are presented as **means ± standard deviations**.

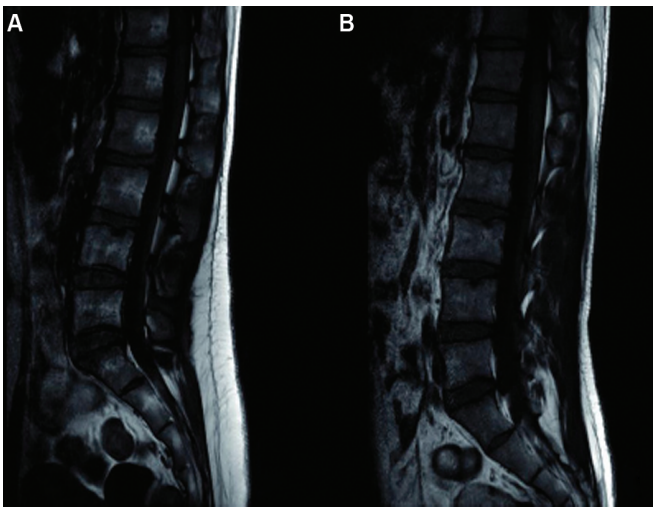

Fig. (2). T1WI of lumbar vertebrae MRI. **A**: T1WI from a SENSE-TSE scan of a 45-year-old male patient who was experiencing low back pain for one week; **B**: T1WI from a CS-TSE scan of a 43-year-old male patient who was experiencing radiating pain to the left lower limb. (*A higher resolution / colour version of this figure is available in the electronic copy of the article*).

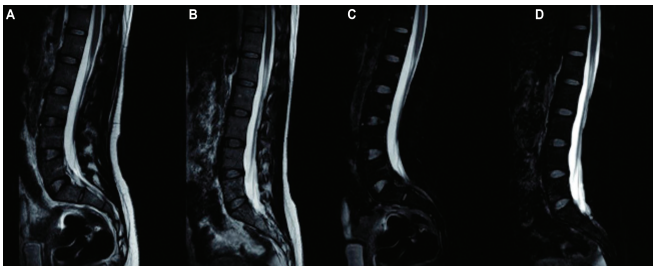

Fig. (3). T2WI and PDWI of lumbar vertebrae MRI. **A** and **C**: T2WI and PDWI from a SENSE-TSE scan of a 35-year-old female patient who was experiencing low back pain for 1 year. **B** and **D**: T2WI and PDWI from a CS-TSE scan of a 40-year-old female patient who was experiencing low back pain for 6 months. (*A higher resolution / colour version of this figure is available in the electronic copy of the article*).

3.2. Subjective Evaluation of Image Quality

Schematic diagrams of SENSE-TSE and CS-TSE are shown in Figs. (**2** and **3**), respectively. The overall quality of T1WI, T2WI, and PDWI images from SENSE-TSE and CS-TSE sequences had median scores of 5 ($p > 0.05$). Subjective evaluations of signal uniformity for bone marrow, muscle, conus medullaris, and nerve root morphology regions in T1WI, T2WI, and PDWI images from SENSE-TSE and CS-TSE also had median scores of 5 ($p > 0.05$). Furthermore, the subjective evaluation of image quality was very consistent between the two radiologists ($\kappa > 0.75$), as shown in Table **4**.

Each radiologist was able to outline the nerve root in the intervertebral foraminal in T1WI sagittal images. In T2WI transverse images, each radiologist evaluated the vagueness and distortion of the anterior, posterior, right, and left edges of nerve roots subjectively. The median score of these evaluations was 5 ($p > 0.05$), as shown in Fig. (**4**).

3.3. Effectiveness of Disease Diagnosis

Among the 300 patients who received CS-TSE, 148 and 136 had centrum lesions ($\kappa = 0.897$), 271 and 269 had intervertebral disc lesions ($\kappa = 0.882$), 15 and 10 had soft tissue lesions ($\kappa = 0.832$), and 61 and 59 had spinal cord lesions ($\kappa = 0.924$), as diagnosed by the two radiologists, respectively (Table **5**).

The degree of intervertebral foraminal stenosis among the 300 patients who received CS-TSE was classified by the two radiologists using Lee's classification method. The classification values assigned by each radiologist, respectively, are as follows: 0 for 24 and 35 cases, 1 for 156 and 125 cases, 2 for 90 and 100 cases, and 3 for 30 and 40 cases ($\kappa = 0.882$), as shown in Fig. (**5**).

The diagnoses made with SENSE-TSE sequences relative to intraoperative diagnoses had Sen, Sep, PV+, and PV- values, respectively as follows: for centrum disease, 86.15%, 92.50%, 90.32%, and 89.16%; for intervertebral disc disease, 98.51%, 80.00%, 98.51%, and 86.96%; for spinal cord disease, 90.00%, 99.25%, 90.00%, and 99.25%;

and for soft tissue lesions, 93.33%, 94.62%, 87.50%, and 99.22%. The diagnoses made with CS-TSE sequences relative to intraoperative diagnoses had Sen, Sep, PV+, and PV- values, respectively, as follows: for centrum disease, 87.14%, 92.31%, 89.71%, and 90.32%; for intervertebral disc disease, 98.67%, 76.92%, 97.99%, and 83.33%; for spinal cord disease, 92.31%, 98.65%, 85.71%, and 99.31%; and for soft tissue lesions, 94.44%, 97.90%, 85.00%, and 99.29% (Table **6**).

4. DISCUSSION

SENSE-TSE is widely used in routine MRI of joints and requires a long scan time. Maintaining the same position for a long time causes discomfort to patients. Consequently, an unwanted movement that degrades image quality can occur. Therefore, shortening the scan time can reduce motion artifacts and is an important goal for the clinical application of CS acceleration [15, 19]. In this study, MR images of the lumbar vertebrae remained acceptable when CS acceleration was incorporated into SENSE-TSE acquisition. Although the scan time was shortened by approximately 40%, the change in overall diagnostic performance was negligible. For patients with chronic low back pain, remaining in a supine position on the imaging table for a long time is difficult, if not impossible. Therefore, CS acceleration would be beneficial for these patients.

Although SENSE-TSE and CS-TSE sequences were not performed in the same patients, we used a large sample size and observed no statistical differences in either gender ratio or age distribution between the SENSE-TSE and CS-TSE groups. Therefore, we believe that the two sets of experimental data are comparable.

Image contrast was not compromised by the iterative-reconstruction process of CS [26]. The CNRs of bone marrow-CSF, muscle-CSF, and spinal cord-CSF in the T2WI and PDWI images from CS-TSE sequences were higher than those from SENSE-TSE sequences. In the objective evaluations of image quality performed by measuring the SNR and CNR, no significant differences were observed ($p > 0.050$). However, the SNRs and CNRs of some regions acquired by CS-TSE were lower than those acquired by SENSE-TSE. The overall image quality of the T1WI and T2WI images from CS-TSE was considered acceptable for routine clinical practice, as shown in Figs. (**2** and **3**). We also analyzed PDWI images without fat suppression. Although fat suppression can enhance the contrast of soft tissue to improve lesion visualization [27, 28], MRI without fat suppression is preferred for identifying normal anatomical structures because fat commonly exists in such structures. SNRs of bone marrow, muscle, and spinal cord regions in PDWI images from CS-TSE sequences were lower than those in PDWI images from SENSE-TSE sequences. However, the differences were not significant ($p > 0.05$), and the image quality was judged acceptable by both radiologists (Fig. **3D**). On the other hand, CNRs of bone marrow-CSF, muscle--CSF, and spinal cord-CSF regions in PDWI images from CS-TSE sequences were higher than those in PDWI images from SENSE-TSE sequences, and the CS-TSE scan time was reduced from 2 min 40 s to 1 min 23 s.

Table 4. Subjective image quality analysis of TSE imaging of lumbar spine without and with CS.

-	T1WI			T2WI			PDWI		
-	SENSE	CS	P-value	SENSE	CS	P-value	SENSE	CS	P-value
Bone marrow	5	5	0.540	5	5	0.862	5	5	0.854
Muscle	5	5	0.741	5	5	0.865	5	5	0.755
Spinal cord	5	5	0.531	5	5	0.871	5	5	0.730
Nerve root	5	5	0.756	5	5	0.823	-	-	-

The data are presented as **median**.

Table 5. Diagnostic agreement for TSE imaging of lumbar spine with CS.

-	Bone Marrow	Discs	Soft Tissue	Spinal Cord
Radiologist 1	148	271	15	61
Radiologist 2	136	269	10	59
Radiologist 3	145	269	13	62
Radiologist 4	140	270	14	58
Kappa-values	0.897	0.882	0.832	0.924

Table 6. Diagnostic accuracy for TSE imaging of lumbar spine without and with CS.

-	Sen		Spe		PV+		PV-	
	SENSE	**CS**	**SENSE**	**CS**	**SENSE**	**CS**	**SENSE**	**CS**
Bone marrow	86.15%	87.14%	92.50%	92.31%	90.32%	89.71%	89.16%	90.32%
Discs	98.51%	98.67%	80.00%	76.92%	98.51%	97.99%	86.96%	83.33%
Spinal cord	90.00%	92.31%	99.25%	98.65%	90.00%	85.71%	99.25%	99.31%
Soft tissue	93.33%	94.44%	94.62%	97.90%	87.50%	85.00%	99.22%	99.29%

Sen = Sensitivity, Spe = Specificity, PV+ = Positive predictive value, PV- = Negative predictive value.

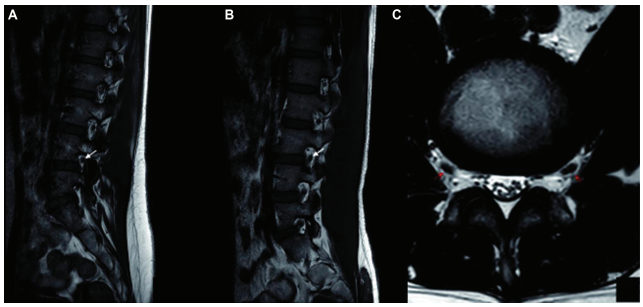

Fig. (4). Nerve root visualization with MRI. **A**: SENSE-TSE-T1WI; **B**: CS-TSE-T1WI; **C**: CS-TSE-T2WI. (*A higher resolution / colour version of this figure is available in the electronic copy of the article*).

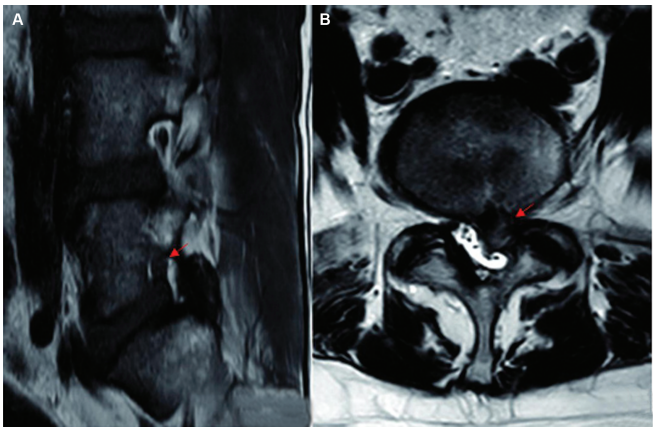

Fig. (5). Intervertebral foraminal stenosis. **A**: Grade 1 foraminal stenosis; **B**: Grade 3 foraminal stenosis. (*A higher resolution / colour version of this figure is available in the electronic copy of the article*).

In this study, we also analyzed the vagueness and deformation of nerve root margins in images from SENSE-TSE and CS-TSE sequences. Only 16 cases in the SENSE-TSE group and 19 cases in the CS-TSE group were assigned a score of 2. Possible reasons for this finding may be the undersampling of k-space and the CS reconstruction algorithm [17], a poor transverse position angle, or the partial volume effect. The morphology and signal uniformity of nerve roots were considered acceptable in the remaining images (median score of 5). The consistency of scoring between the two radiologists was also high ($\kappa = 0.618$), as shown in Fig. (**4**). In T1WI images from SENSE-TSE and CS-TSE sequences, the image quality ratings of the two reviewers were very similar for the contours of nerve roots where no CSF was present in the background (Fig. **4B**).

In addition to quantitative measurement of image quality by SNR and CNR, evaluation of diagnostic accuracy is also important. In diagnosing lesions of the lumbar vertebrae, intervertebral discs, spinal cord, and soft tissue, there was high consistency between the two radiologists using CS-TSE sequences (all κ values were > 0.75). Evaluations of the degree of lumbar foraminal stenosis and nerve root compression using CS-TSE sequences were also consistent ($\kappa = 0.882$). Patients diagnosed as having grade 3 foraminal lumbar stenosis and nerve root compression (Fig. **5**) all exhibited clinical symptoms of low back pain and pain radiating to a lower limb, suggesting that the potential of CS-TSE for accurately diagnosing lumbar vertebral diseases is high. There were no significant differences in the values of Sen, Sep, PV+, and PV- between the SENSE-TSE and CS-TSE groups.

Setting the CS acceleration factor for CS-TSE depends on the signal source, the size of the imaging matrix, and the number of channels in the RF receiving coils. The size of the imaging matrix determines the k-space undersampling pattern. The number of channels number in the receiving coils determines the amount of acquirable data that can be incorporated into the reconstruction process [29, 30]. A multi-channel coil can also acquire data with high SNRs, resulting in improved image quality or allowing the scan time to be shortened [31]. A 44-channel posterior coil was used in this study to achieve high SNRs and CS acceleration. Increasing the CS acceleration factor can reduce the scan time, but too substantial an increase can degrade the image quality. Therefore, it is important to optimize the CS acceleration factor for each sequence and each anatomical location based on the available RF coils before CS-TSE is widely used in clinical practice.

CONCLUSION

This study has several limitations. Firstly, the study is retrospective; therefore, paired experiments could not be conducted, and individual differences were not considered. To compensate for this limitation, the number of cases was increased. Secondly, default CS acceleration factors of the system were used. Optimal CS acceleration factors for different

diagnostic purposes need to be determined experimentally, which is the goal of a separate ongoing project. Thirdly, surgical observations were not available as a reference to evaluate the diagnoses determined from images.

This retrospective study showed that a combination of compressed SENSE and TSE is a tool for diagnosing lumbar vertebrae and intervertebral disc disease that provides image quality and diagnostic consistency equivalent to that of SENSE-TSE, with reduced imaging time. The reduction in imaging time could improve patient comfort, accelerate patient throughput, and acquire more data at a higher resolution to diagnose vertebral lesions, intervertebral disc and spinal canal diseases, and soft tissue lesions.

ETHICS APPROVAL AND CONSENT TO PARTICIPATE

This study was approved by the Ethics Committee of Shengjing Hospital of China Medical University, China [Approval number: 2019PS444K].

HUMAN AND ANIMAL RIGHTS

No animals were used in this study. All the human procedures were is in accordance with the ethical standards of the committee responsible for human experimentation (institutional and national), and with the Helsinki Declaration of 1975, as revised in 2013 (http://ethics.iit.edu/ecodes/node/3931)

CONSENT FOR PUBLICATION

The requirement for informed consent was waived.

AVAILABILITY OF DATA AND MATERIALS

Due to the nature of this research, participants of this study did not agree for their data to be shared publicly, so supporting data is not available.

FUNDING

This work was financially supported by the National Natural Science Foundation of China (No. 30871211, No. 81271538) and 345 Talent Project and Natural Science Foundation of Liaoning Province [No. 2019-ZD-0794].

CONFLICT OF INTEREST

The authors declare no conflict of interest, financial or otherwise.

ACKNOWLEDGEMENTS

Declare none.

REFERENCES

[1] Goceri N, Goceri E. A Neural Network Based Kidney Segmentation from MR Images. Miami, Florida, USA: The 14th IEEE International Conference on Machine Learning and Applications. 1195-8.
http://dx.doi.org/10.1109/ICMLA.2015.229

[2] Goceri E. Automatic Kidney Segmentation Using Gaussian Mixture Model on MRI Sequences. In: Wan X. (eds) Electrical Power Systems and Computers. Lecture Notes in Electrical Engineering, 2011; vol 99. Springer, Berlin, Heidelberg..
http://dx.doi.org/10.1007/978-3-642-21747-0_4

[3] Goceri E. A comparative evaluation for liver segmentation from spir images and a novel level set method using signed pressure force function. Izmir: Izmir Institute of Technology 2013.

[4] Goceri E, Songul C. Biomedical Information Technology: Image Based Computer Aided Diagnosis Systems. Antalya, Turkey Int Conf on Advanced Technologies.

[5] Goceri E. Automatic labeling of portal and hepatic veins from MR images prior to liver transplantation. Int J CARS 2016; 11(12): 2153-61.
http://dx.doi.org/10.1007/s11548-016-1446-8 PMID: 27338273

[6] Goceri E, Shah ZK, Gurcan MN. Vessel segmentation from abdominal magnetic resonance images: adaptive and reconstructive approach. Int J Numer Methods Biomed Eng 2017; 33(4): Epub 2016 Aug 2.
http://dx.doi.org/10.1002/cnm.2811 PMID: 27315322

[7] Feng L, Benkert T, Block KT, Sodickson DK, Otazo R, Chandarana H. Compressed sensing for body MRI. J Magn Reson Imaging 2017; 45(4): 966-87.
http://dx.doi.org/10.1002/jmri.25547 PMID: 27981664

[8] Pillastrini P, Gardenghi I, Bonetti F, *et al.* An updated overview of clinical guidelines for chronic low back pain management in primary care. Joint Bone Spine 2012; 79(2): 176-85.
http://dx.doi.org/10.1016/j.jbspin.2011.03.019 PMID: 21565540

[9] Pruessmann KP, Weiger M, Scheidegger MB, Boesiger P. SENSE: sensitivity encoding for fast MRI. Magn Reson Med 1999; 42(5): 952-62.
http://dx.doi.org/10.1002/(SICI)1522-2594(199911)42:5<952::AID-MRM16>3.0.CO;2-S PMID: 10542355

[10] David LD. Compressed sensing. IEEE Trans Inf 2006; 52: 1289-306.
http://dx.doi.org/10.1109/TIT.2006.871582

[11] Lustig M, Donoho D, Pauly JM. Sparse MRI: The application of compressed sensing for rapid MR imaging. Magn Reson Med 2007; 58(6): 1182-95.
http://dx.doi.org/10.1002/mrm.21391 PMID: 17969013

[12] Jaspan ON, Fleysher R, Lipton ML. Compressed sensing MRI: a review of the clinical literature. Br J Radiol 2015; 88(1056): 20150487.
http://dx.doi.org/10.1259/bjr.20150487 PMID: 26402216

[13] Zhang T, Chowdhury S, Lustig M, *et al.* Clinical performance of contrast enhanced abdominal pediatric MRI with fast combined parallel imaging compressed sensing reconstruction. J Magn Reson Imaging 2014; 40(1): 13-25.
http://dx.doi.org/10.1002/jmri.24333 PMID: 24127123

[14] Liu F, Duan Y, Peterson BS, Kangarlu A. Compressed sensing MRI combined with SENSE in partial k-space. Phys Med Biol 2012; 57(21): N391-403.
http://dx.doi.org/10.1088/0031-9155/57/21/N391 PMID: 23073235

[15] Bratke G, Rau R, Weiss K, *et al.* Accelerated MRI of the Lumbar spine using compressed sensing: Quality and efficiency. J Magn Reson Imaging 2018 2019; 49(7): e164-75.
PMID: 30267462

[16] Altahawi FF, Blount KJ, Morley NP, Raithel E, Omar IM. Comparing an accelerated 3D fast spin-echo sequence (CS-SPACE) for knee 3-T magnetic resonance imaging with traditional 3D fast spin-echo (SPACE) and routine 2D sequences. Skeletal Radiol 2017; 46(1): 7-15.
http://dx.doi.org/10.1007/s00256-016-2490-8 PMID: 27744578

[17] Yi J, Lee YH, Hahn S, Albakheet SS, Song H-T, Suh J-S. Fast isotropic volumetric magnetic resonance imaging of the ankle: Acceleration of the three-dimensional fast spin echo sequence using compressed sensing combined with parallel imaging. Eur J Radiol 2019; 112: 52-8.
http://dx.doi.org/10.1016/j.ejrad.2019.01.009 PMID: 30777219

[18] Kijowski R, Rosas H, Samsonov A, King K, Peters R, Liu F. Knee imaging: Rapid three-dimensional fast spin-echo using compressed sensing. J Magn Reson Imaging 2017; 45(6): 1712-22.
http://dx.doi.org/10.1002/jmri.25507 PMID: 27726244

[19] Lee SH, Lee YH, Song H-T, Suh J-S. Rapid acquisition of magnetic resonance imaging of the shoulder using three-dimensional fast

spin echo sequence with compressed sensing. Magn Reson Imaging 2017; 42: 152-7.
http://dx.doi.org/10.1016/j.mri.2017.07.022 PMID: 28751204

[20] Uecker M, Lai P, Murphy MJ, *et al.* ESPIRiT- an eigenvalue approach to autocalibrating parallel MRI: where SENSE meets GRAPPA. Magn Reson Med 2014; 71(3): 990-1001.
http://dx.doi.org/10.1002/mrm.24751 PMID: 23649942

[21] Hu Y, Pan S, Zhao X, Guo W, He M, Guo Q. Value and clinical application of orthopedic metal artifact reduction algorithm in CT scans after orthopedic metal implantation. Korean J Radiol 2017; 18(3): 526-35.
http://dx.doi.org/10.3348/kjr.2017.18.3.526 PMID: 28458605

[22] Lee S, Lee JW, Yeom JS, *et al.* A practical MRI grading system for lumbar foraminal stenosis. AJR Am J Roentgenol 2010; 194(4): 1095-8.
http://dx.doi.org/10.2214/AJR.09.2772 PMID: 20308517

[23] Schizas C, Theumann N, Burn A, *et al.* Qualitative grading of severity of lumbar spinal stenosis based on the morphology of the dural sac on magnetic resonance images. Spine 2010; 35(21): 1919-24.
http://dx.doi.org/10.1097/BRS.0b013e3181d359bd PMID: 20671589

[24] Xiong X, Zhou Z, Figini M, Shangguan J, Zhang Z, Chen W. Multi-parameter evaluation of lumbar intervertebral disc degeneration using quantitative magnetic resonance imaging techniques. Am J Transl Res 2018; 10(2): 444-54.
PMID: 29511438

[25] Urrutia J, Besa P, Campos M, *et al.* The Pfirrmann classification of lumbar intervertebral disc degeneration: an independent inter- and intra-observer agreement assessment. Eur Spine J 2016; 25(9): 2728-33.
http://dx.doi.org/10.1007/s00586-016-4438-z PMID: 26879918

[26] Fritz J, Raithel E, Thawait GK, Gilson W, Papp DF. Six-fold acceleration of high-spatial resolution 3D SPACE MRI of the knee through incoherent k-Space undersampling and iterative reconstruction-first experience. Invest Radiol 2016; 51(6): 400-9.
http://dx.doi.org/10.1097/RLI.0000000000000240 PMID: 26685106

[27] Delfaut EM, Beltran J, Johnson G, Rousseau J, Marchandise X, Cotten A. Fat suppression in MR imaging: techniques and pitfalls. Radiographics 1999; 19(2): 373-82.
http://dx.doi.org/10.1148/radiographics.19.2.g99mr03373 PMID: 10194785

[28] Lee S-Y, Jee W-H, Kim SK, Kim J-M. Proton density-weighted MR imaging of the knee: fat suppression versus without fat suppression. Skeletal Radiol 2011; 40(2): 189-95.
http://dx.doi.org/10.1007/s00256-010-0969-2 PMID: 20512570

[29] Hollingsworth KG. Reducing acquisition time in clinical MRI by data undersampling and compressed sensing reconstruction. Phys Med Biol 2015; 60(21): R297-322.
http://dx.doi.org/10.1088/0031-9155/60/21/R297 PMID: 26448064

[30] de Zwart JA, Ledden PJ, van Gelderen P, Bodurka J, Chu R, Duyn JH. Signal-to-noise ratio and parallel imaging performance of a 16-channel receive-only brain coil array at 3.0 Tesla. Magn Reson Med 2004; 51(1): 22-6.
http://dx.doi.org/10.1002/mrm.10678 PMID: 14705041

[31] Link TM. MR imaging in osteoarthritis: hardware, coils, and sequences. Radiol Clin North Am 2009; 47(4): 617-32.
http://dx.doi.org/10.1016/j.rcl.2009.04.002 PMID: 19631072